Mechanical metamaterials: Toughness and design criteria

February 21 2022, by Thamarasee Jeewandara

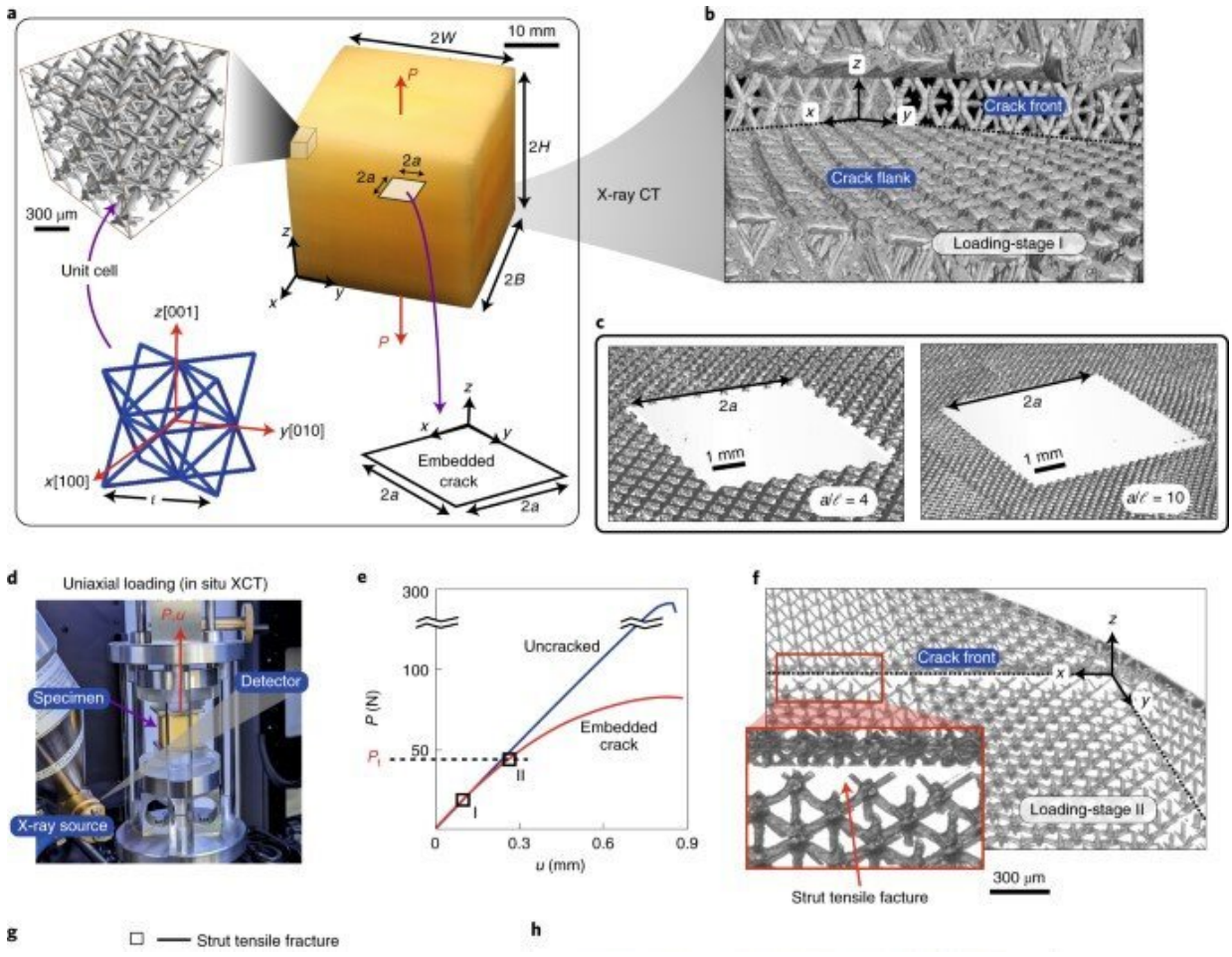

Failure under uniaxial tensile loading. (a) Optical image of the cubic octet-truss specimen with an embedded square crack of side 2a. Insets: XCT images of the octet-truss microstructure, unit cell and orientation and geometry of the embedded crack. b,c, XCT images of the crack front/flank at loading-stage I in e (b) and cracks of fixed size 2a but with varying cell sizes ℓ as parameterized by

a/ℓ (c). d, Tensile loading set-up, with in situ XCT imaging. e, Tensile load P versus displacement u response of the $\bar{\rho}$=0.08 uncracked and cracked (a/ℓ=10) specimens. f, The crack front/flanks at KIc (loading-stage II in e). Inset: a magnified view of the failed crack front struts. g, Measured normalized toughness $\bar{K}$Ic versus relative density $\bar{\rho}$ (lines are FE predictions and symbols are measurements with error bars indicating variation over five test samples). h, XCT image for the $\bar{\rho}$ = 0.03 and a/ℓ=4 specimen when failure is set by elastic buckling of crack front struts Inset: a magnified view of the buckled struts. Nature Materials, https://doi.org/10.1038/s41563-021-01182-1

Mechanical metamaterials are an emerging class of materials primarily governed by their architecture to create lightweight materials with extreme mechanical properties. The functionality of such materials is limited by their tolerance to damage and defects, better known as "fracture toughness." Materials scientists credit the difficulty in part to the manufacture and characterization of a large number of unit cells. In a recent report now published on *Nature Materials*, Angkur Jyoti Dipanka Shaikeea and a team of scientists in engineering and metamaterials at the University of Cambridge U.K., and the University of California, Los Angeles, U.S., combined numerical and asymptotic analyses to extend the ideas of elastic fracture mechanics to mechanical 3D metamaterials and developed a design protocol to form optimally robust discrete solids.

The evolution of materials

The evolution of materials engineering has led to the development of a range of material properties with unique combinations, and the material property space can be expanded by introducing new alloys and new microstructures. Advances in additive manufacture have allowed intriguingly accurate small-scale, periodic and functionally graded architectures that can be formed into large networks to create man-made materials on the macroscopic scale known as metamaterials, alongside

mechanical metamaterials more distinctly defined by their structure rather than composition.

Three-dimensional (3D) micro- and nano-lattices are a promising class of low-density materials with numerous applications including thermal insulation and energy absorption, with remarkable mechanical and functional properties. These functionalities are governed by the parent material and their architecture, known as mechanical metamaterials. Researchers have used additive manufacturing methods, including projection microstereolithography and two-photon lithography to form polymeric, metallic and ceramic metamaterials.

Primary author Angkur Shaikeea is a Cambridge India Ramanujan Scholar; he joined Cambridge for his Ph.D. with Professor Vikram Deshpande, who is an eminent scholar in mechanics of solids. Shaikeea is currently the Ashby Research Fellow in the Engineering department at Cambridge. The team of scientists have formed key collaborations with another leading team at the metamaterial fabrication lab of Dr. Xiaoyu Rayne Zheng at the University of California, Los Angeles, U.S., to realize the outcomes of this research. In this work, Shaikeea et al. used a stretch-dominated metamaterial made of a network of struts to form an octet-truss. The team developed the large 3D specimens containing nearly 10 million periodic cells and cell sizes as small as 150 μm via large-area projection microstereolithography to form each layer through a continuously moving projection via subsections.

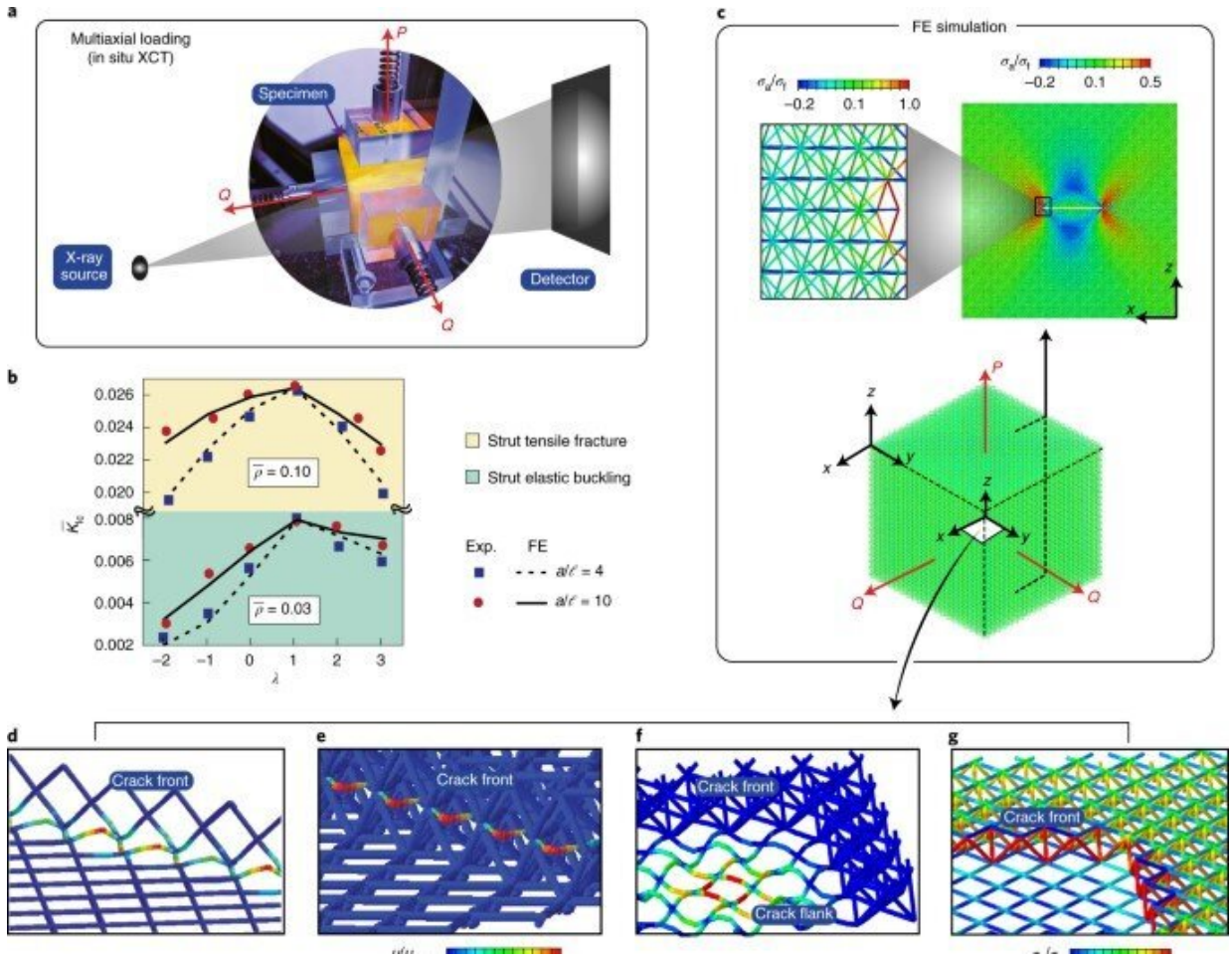

Failure under multiaxial loading. (a) Multiaxial loading set-up with in situ XCT imaging. (b) Summary of the measurements and FE predictions of $K^{-}Ic$ as a function of the load triaxiality $\lambda \equiv Q/P$ for specimens that fail by strut fracture ($\rho^{-} = 0.1$) and elastic strut buckling ($\rho^{-} = 0.03$). Results are shown for two values of a/ℓ in both cases. (c) FE modelling of the specimens. Insets: individual struts modelled as elastic solids and shaded by contours of the normalized axial stress $\sigma a/\sigma f$ (σf is the strength of the parent solid TMPTA). (d–f) FE predictions of the failure modes for loading with $\lambda = 1$. Failure set by elastic buckling of crack front (d,e) and crack flank struts (f) of the $\rho^{-}=0.03$ and $a/\ell=4$ specimen. The predicted $K^{-}Ic$ differs by 1% between the different eigenmodes in d and e, and by 2% between e and f. The struts are shaded by magnitude of normalized displacement u/umax. g, Distribution of normalized axial stresses $\sigma a/\sigma f$ for the $a/\ell=10$ and $\rho^{-}=0.10$ specimen ($\lambda = 1$) with crack tip struts predicted to undergo tensile fracture at KIc. h,i, XCT images for the $\rho^{-}=0.03$ and $a/\ell=4$ specimen for

loading with λ = 1 when failure is set by elastic buckling of crack front struts (h) and crack flank struts (i). Insets: magnified views of the buckled struts. The measured KIc between h and i differs by only 2%. Nature Materials, https://doi.org/10.1038/s41563-021-01182-1

Cutting-edge experimental methods

The experimental system allowed the scientists to manufacture samples with embedded cracks to perform a range of valid fracture toughness measurements. Using in situ X-ray computed tomography and large-scale numerical simulations, the team characterized fracture mechanisms across a range of specimen densities, parent materials, cell sizes and crack sizes, including loading configurations. Shaikeea described the concept of architected metamaterials as "a rapidly proliferating engineering material suited for a wide range of applications, although such materials are limited in structural applications simply since, no engineering material can find application without a clear understanding of defect and damage tolerance." He explained that "this was highlighted thus far by a lack of experiments measuring the toughness in large 3D specimens."

To generate the required crack-tip K field for fracture toughness mechanisms, they formed the metamaterial specimen by using a large-area projection microstereolithography system. The method allowed printing of each layer via single projection to develop inhomogeneous material properties, although with enclosed heat in the central region. To overcome this, the team used a moving projection system for curing in subsections for reduced heat generation with enhanced dissipation, and increased printing area without sacrificing resolution.

The team combined the experimental setup with X-ray computed

tomographic (XCT) observations and large-scale numerical simulations to characterize fracture mechanics of truss-based 3D metamaterials. Shaikeea notes the use of "XCT data as a major advancement for experimental mechanics in general." As a first step to characterize the fracture, they employed uniaxial tensile tests, and combined them with an in situ observation protocol. To develop a physical understanding of the observations, they performed finite element simulations for uniaxial and multiaxial loading cases and modeled every strut in the specimen.

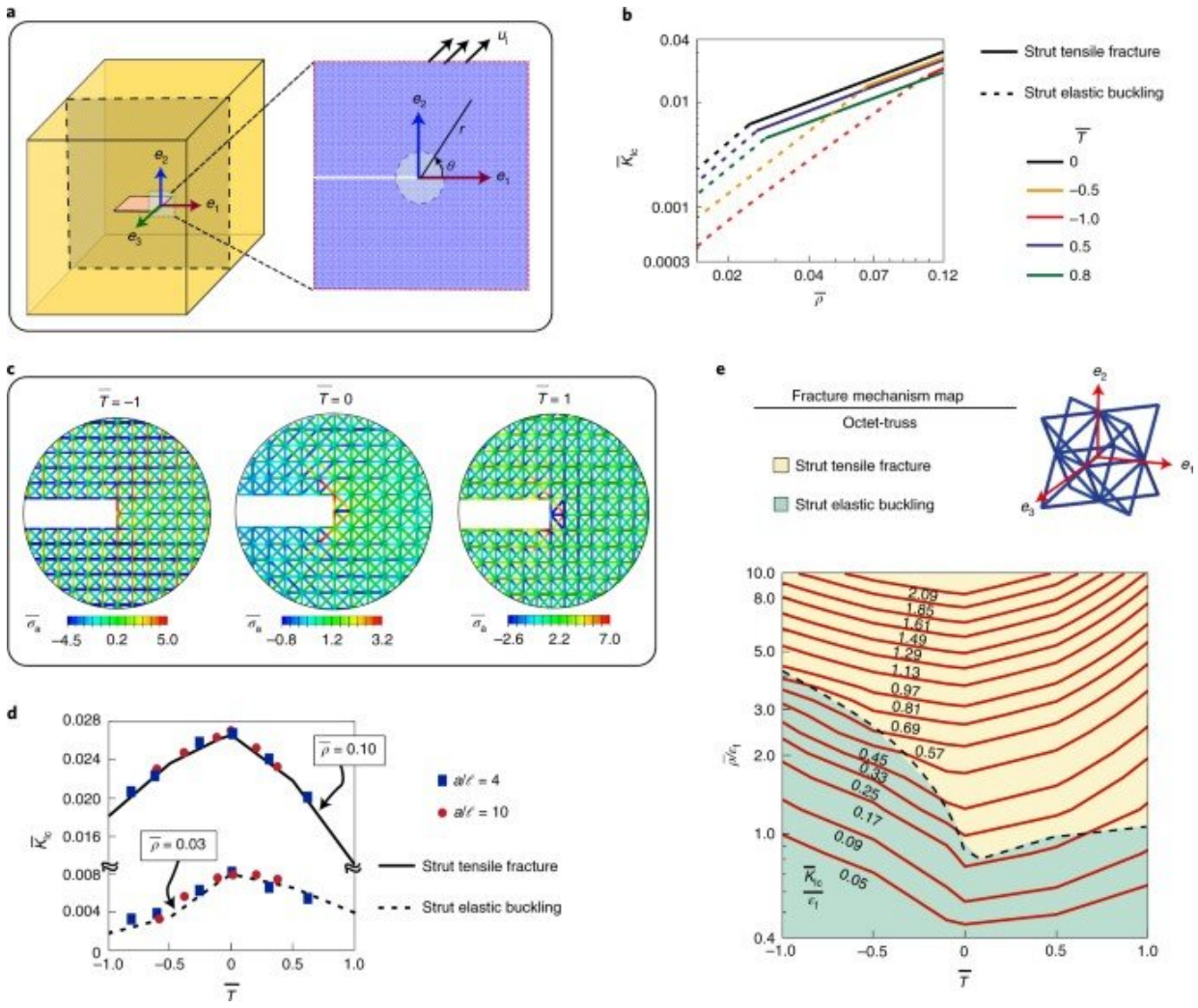

Fracture mechanism map. (a) Sketch illustrating the crack front coordinate system and a 2D slice used in the asymptotic analysis. (b) FE predictions

showing the sensitivity of the asymptotic predictions of $K^{-}Ic$ to T^{-} over a range of relative densities ρ^{-}. (c) FE predictions of normalized axial stress $\sigma^{-}a \equiv \sigma a/(Es\rho^{-})$ around the crack tip for an applied $KI/(Es\ell\sqrt{})=0.01$ and three choices of the normalized T-stress T^{-}. (d) FE predictions and measurements from Fig. 2b replotted as a function of T^{-} to illustrate that ρ^{-} and T^{-} set $K^{-}Ic$, with the effect of a/ℓ and λ both captured within T^{-}. (e) Fracture mechanism map of the octet-truss metamaterial, with axes of normalized T-stress T^{-} and $\rho^{-}/\varepsilon f$ and contours of $K^{-}Ic/\varepsilon f$. The strut tensile fracture and strut elastic buckling failure regimes are shaded. Nature Materials, https://doi.org/10.1038/s41563-021-01182-1

Developing a design protocol: Fracture mechanism maps

The team developed a protocol to select the optimal topology for a given application. They combined calibration factors with metamaterial microstructural parameters and constituent material properties to form "fracture mechanism maps" to provide information on the failure mode and toughness of the metamaterial. By using fracture maps from different types of unit cell topology, they created topology selection maps to maximize toughness or failure loads, allowing researchers to select optimized metamaterial topologies based on various design parameters.

The procedure was independent of topology and is applicable for other classes of truss-based metamaterials. Such maps can be used by materials designers to identify failure in different applications at minimal computational cost, compared to modeling microstructural detail of the metamaterial. This setup can provide a materials selection protocol for mechanical metamaterials design, much like Ashby plots for materials selection in materials design with conventional materials.

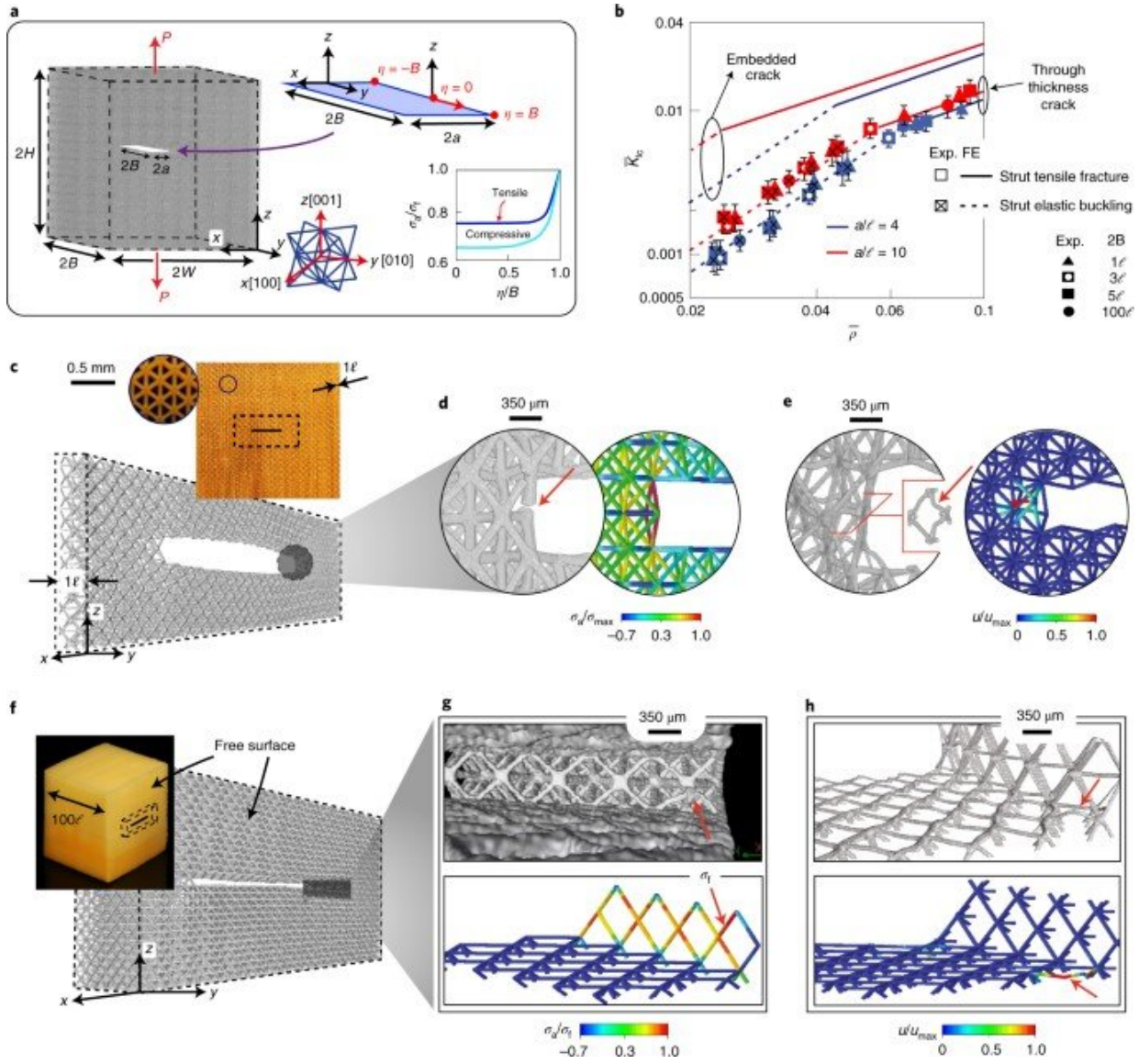

Through-thickness cracks. (a) Sketch illustrating tensile loading of a specimen of thickness 2B with a through-thickness crack (CCT geometry). FE predictions of the variation of normalized axial strut stresses σa/σmax for struts along the crack front (the maximum tensile and compressive stresses are plotted in each unit cell along the crack front) are included in the inset, which also illustrates the local axis η along the crack front with η = 0 at the midplane of the specimen and η = ±B on the specimen free surfaces. b, FE predictions and measurements (error bars indicating variation over five tests) of $K^{-}Ic$ versus ρ^{-} for specimens of different thicknesses 2B. In each case, the results are shown for two values of a/ℓ, with the embedded crack results reproduced from Fig. 1g. c, XCT image of

a portion of the 2B=ℓ specimen. Inset: optical image of the specimen along with a magnified view of the microstructure (scale bar refers to inset). d,e, XCT images and FE predictions of the crack tip state at KIc in the a/ℓ=10 specimen illustrating the tensile fracture ($\rho^- = 0.10$) (d) and elastic strut buckling ($\rho^- = 0.03$) (e) failure modes. The FE predictions show distributions of the normalized axial stress σa/σmax and the normalized displacements u/umax in d and e, respectively, with the maximum taken over all struts in the specimen. f, XCT image of a portion of the 2B=100ℓ specimen, with a/ℓ=10 showing the free surface and five unit cells along the thickness. Inset: optical image of the specimen with the dashed cuboid marking the region of the XCT image. g,h, The corresponding FE predictions and XCT observations show that failure by tensile strut fracture (ρ^-=0.10) (g) and elastic strut buckling (ρ^-=0.03) (h) occurs on the specimen free surfaces. Nature Materials, https://doi.org/10.1038/s41563-021-01182-1

Applications of the proposed framework

The researchers showed that the framework applies to any 3D metamaterial, regardless of its topology and constituent material properties. Further investigations will shed light on the types of constituent material behavior, including stress, which can influence qausibrittle materials. Many engineering materials are affected by strain rates and size effects, where materials that are brittle at bulk scale show improved ductility and toughness at sub-micron scales. The multiscale in situ characterization studies can help understand and predict mechanical properties of the metamaterials with features spanning several orders of magnitude.

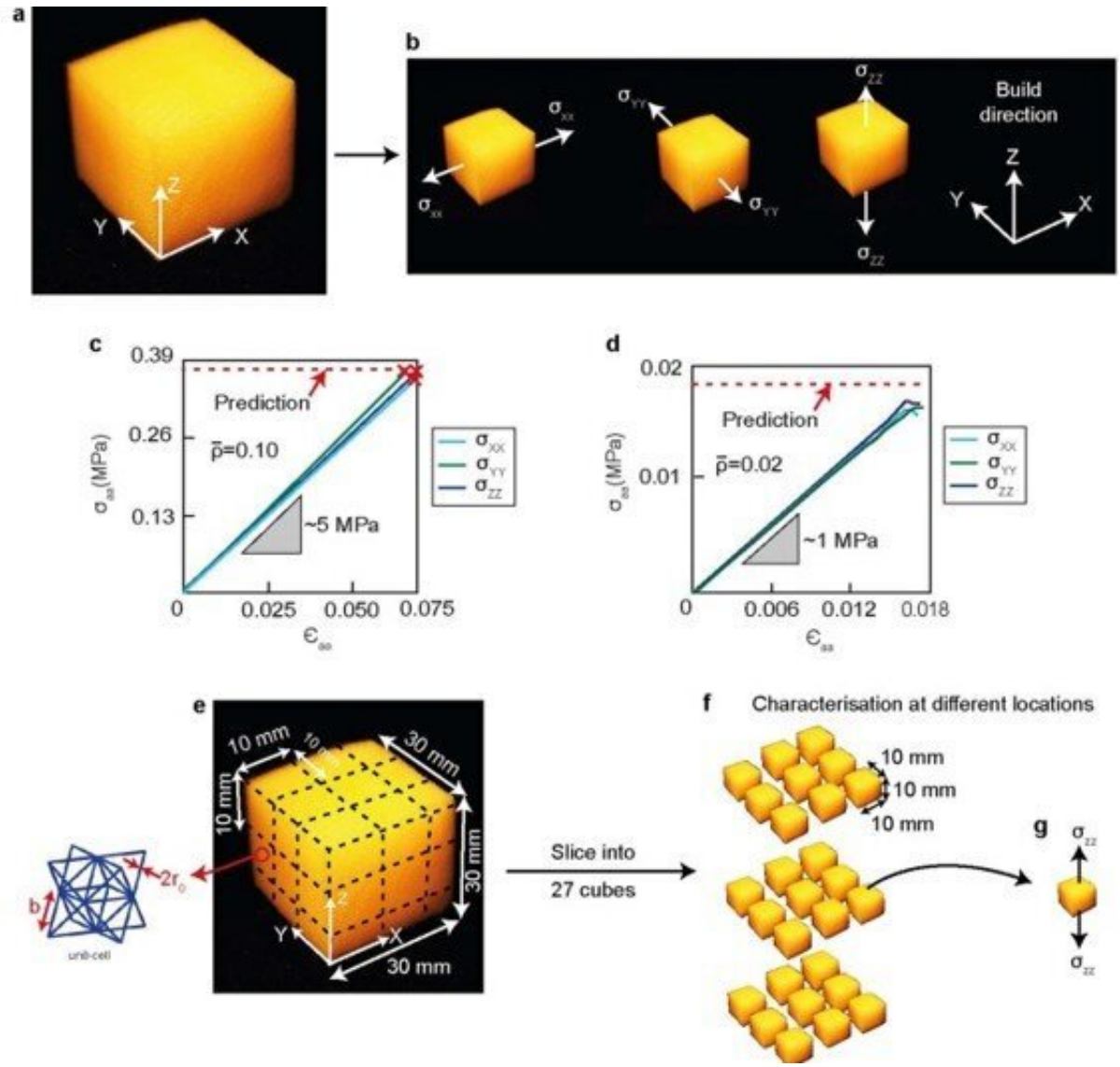

Uniformity of mechanical properties. (a) Optical image of the printed specimen and (b) sketches depicting tensile testing along x, y and z– directions where z is the build direction. The measured tensile responses for the (c) $\rho^- = 0.1$ and (d) $\rho^- = 0.02$ specimens in the x, y and z– directions. Predictions based on the measured properties of a single strut (Supplementary Fig. 2) are included in (c) and (d). (e) The specimen cut into 27 sub-cubes and (f) uniaxial tensile tests were conducted on each cube along the (g) z– direction. The measured responses are shown in (h) and (i) for the $\rho^- = 0.1$ specimen with two different choices of unit cell dimensions. The shaded zone depicts the variation over the 27 sub-cubes with the solid line the mean measured response. Nature Materials, https://doi.org/10.1038/s41563-021-01182-1

The work will inspire investigations of diverse metamaterial topologies including shell and plate lattices, non-uniform periodic arrangements including crystal-inspired architectures. Shaikeea highlights a key outcome of the study as "understanding T-stress and its effects in fracture mechanics of 3D architected solids."

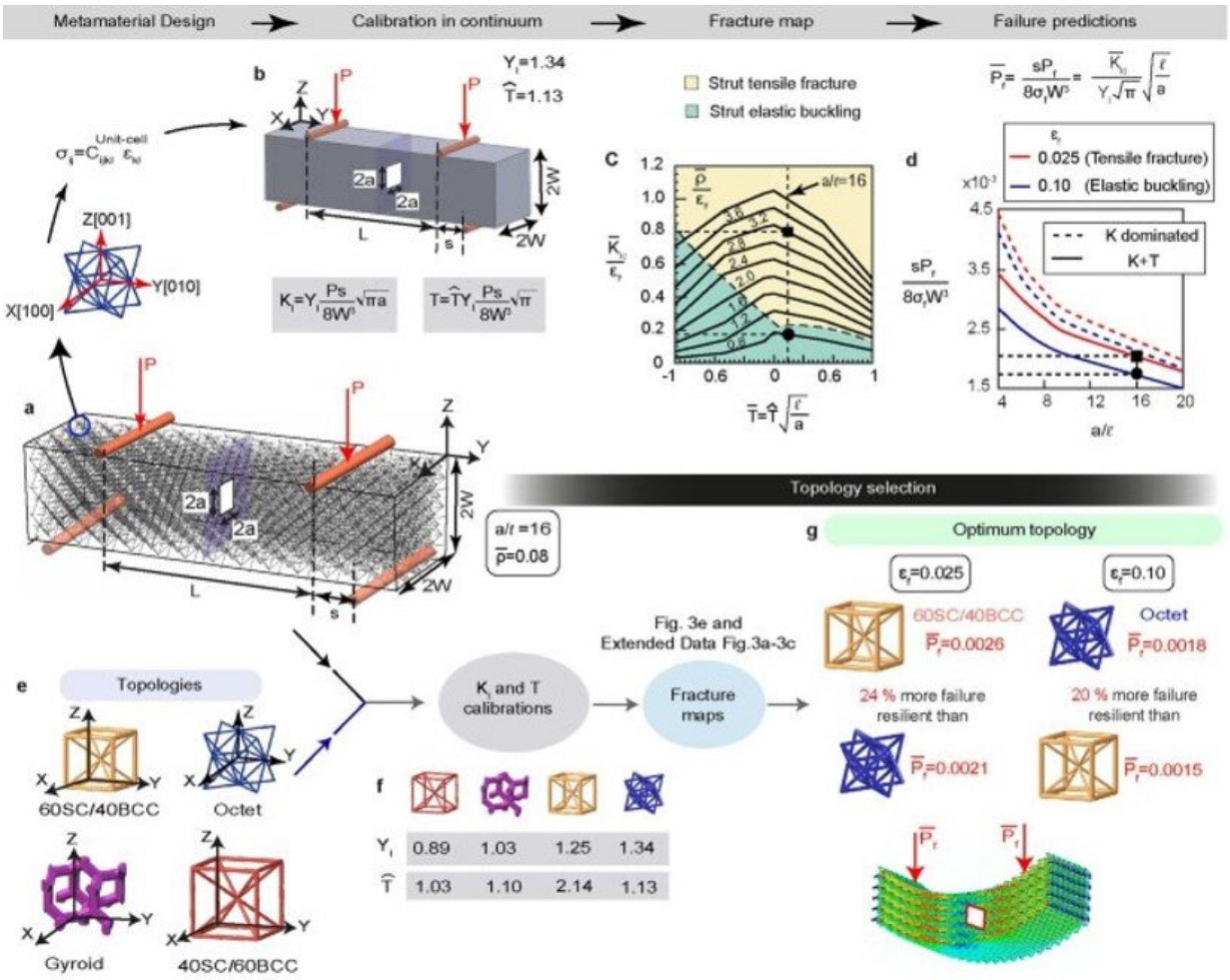

Design with metamaterials. (a) Octet-truss beam of aspect ratio L/W = 20 with the embedded crack (a/W = 0.2) subjected to four-point bending. (b) Geometry of the continuum anisotropic elastic beam used to determine the calibration factors YI and T^ for KIand T, respectively. (c) The cross-plotted fracture map from Fig. 3e. (d) Prediction of the normalized failure load P̄f of the ρ⁻ = 0.08

octet-truss over a range of crack sizes and two choices of parent materials. The reference prediction for an assumed $T^{-}= 0$ is also included. The black markers in (c-d) show examples of the prediction of the normalized failure load P = Pf for a crack with $a/\ell=16$ in a $\rho^{-} = 0.08$ octet-truss metamaterial beam made from parent materials with εf = 0.025 and 0.1. (e-g) Topology selection for maximizing failure load under four-point bending. (e) The four candidate topologies with their orientations labelled in the global beam co-ordinate system (X,Y,Z). (f) Continuum calibration of the geometric constants YI and T^ and (g) description of the optimal topology and improvement over the next best candidate for a $\rho^{-} = 0.08$ beam made from a parent material with failure strains εf = 0.025 and 0.1. Nature Materials, https://doi.org/10.1038/s41563-021-01182-1

Outlook

In this way, Angkur Jyoti Dipanka Shaikeea and colleagues developed a novel study as a milestone towards structural applications of mechanical metamaterials. The work will prompt materials scientists to revisit fundamental concepts of fracture in discrete solids, while providing a framework to form optimal metamaterials for specific applications. More research could be done to explore various topologies, material behaviors and size effects of metamaterials relative to mechanical characteristics of strength and toughness. The work has the potential to develop metamaterial selection maps and performance indices, much like Ashby plots for conventional materials, with profound impact on future mechanical studies.

More information: Angkur Jyoti Dipanka Shaikeea et al, The toughness of mechanical metamaterials, *Nature Materials* (2022). DOI: 10.1038/s41563-021-01182-1

A. Fleck et al, Micro-architectured materials: past, present and future,

Proceedings of the Royal Society A: Mathematical, Physical and Engineering Sciences (2010). DOI: 10.1098/rspa.2010.0215